LETTER

https://doi.org/10.1038/s41586-018-0458-7

Sorting ultracold atoms in a three-dimensional optical lattice in a realization of Maxwell's demon

Aishwarya Kumar[1], Tsung-Yao Wu[1], Felipe Giraldo[1] & David S. Weiss[1]*

In 1872, Maxwell proposed his famous 'demon' thought experiment[1]. By discerning which particles in a gas are hot and which are cold, and then performing a series of reversible actions, Maxwell's demon could rearrange the particles into a manifestly lower-entropy state. This apparent violation of the second law of thermodynamics was resolved by twentieth-century theoretical work[2]: the entropy of the Universe is often increased while gathering information[3], and there is an unavoidable entropy increase associated with the demon's memory[4]. The appeal of the thought experiment has led many real experiments to be framed as demon-like. However, past experiments had no intermediate information storage[5], yielded only a small change in the system entropy[6,7] or involved systems of four or fewer particles[8–10]. Here we present an experiment that captures the full essence of Maxwell's thought experiment. We start with a randomly half-filled three-dimensional optical lattice with about 60 atoms. We make the atoms sufficiently vibrationally cold so that the initial disorder is the dominant entropy. After determining where the atoms are, we execute a series of reversible operations to create a fully filled sublattice, which is a manifestly low-entropy state. Our sorting process lowers the total entropy of the system by a factor of 2.44. This highly filled ultracold array could be used as the starting point for a neutral-atom quantum computer.

With an eye towards quantum computing and quantum simulation applications, there has been a recent boom in cold-atom sorting experiments. Atoms in a variety of arrays of dipole light traps have been impressively rearranged by moving individual traps[6,7,11,12]. The entropy associated with disordered occupancy in those cases is at most about 10% of the system entropy[6], which is dominated by vibrational excitation in the traps. Good vibrational cooling, along with well-sorted atoms, is required for cold collision-based quantum gates or quantum simulations. For Rydberg-based gates or simulations[13], although atoms are not strictly required to be vibrationally cold, colder is better. Rydberg gates using colder atoms are likely to yield higher fidelity because the atoms are less likely to change vibrational states during the gate, which can undesirably entangle atomic motion with qubit states. In general, better-localized atoms allow higher-fidelity addressing of individual atoms[14]. In blue-detuned traps, cold atoms see less light and thus scatter fewer trapping photons, which leads to longer coherence times. For instance, the coherence time in our experiment now exceeds 12 s.

Four atoms in a one-dimensional optical lattice[8] have been compacted using a method[15] similar to the one that we demonstrate here with 50 atoms in three dimensions. We note that at least about 50 qubits are needed for a quantum computer to perform a calculation that cannot be accomplished on a classical computer[16]. A three-dimensional (3D) geometry gives atoms many more nearby neighbours, which provides higher connectivity in the system. It also allows for a broad range of quantum simulations and is favourable for further scaling of the number of atoms in the system.

Our experiment proceeds as follows. We prepare a randomly 56%-filled blue-detuned 3D lattice with 4.8 μm lattice spacing[17]. By imaging polarization-gradient-cooling laser light, we determine the occupancy across the lattice with an error of 10^{-3} per site in 800 ms (ref. [17]). Projection sideband cooling[18] puts 89% of the caesium atoms into their vibrational ground states and >99.7% of them in the $|F=4, m_F=-4\rangle$ hyperfine ground state, where F and m_F are the hyperfine and magnetic quantum numbers, respectively. We then combine the ability to address atoms at individual sites (by using crossed laser beams and microwaves to make site-dependent state changes[19]) with the ability to make state-dependent lattice translations (by rotating the lattice beam polarizations[20]). Starting from a given 3D occupancy map we devise a sequence of operations to fill up either a $5 \times 5 \times 2$ or a $4 \times 4 \times 3$ sublattice.

We can target any site in a $5 \times 5 \times 5$ lattice by using a pair of focused addressing beams intersecting at a right angle[14,19]. Targeting proceeds as in our previous demonstration of high-fidelity single-qubit gates[14], but the magnetic sublevels are different and in this case we are unconcerned with long-term quantum coherence. The addressing beams shift the ($|F=4, m_F=-4\rangle$ to $|F=3, m_F=-3\rangle$ resonance by around 50 kHz, which allows us to drive the associated microwave transition using an adiabatic fast-passage pulse (see Methods for details) that transfers only the target atom. An atom making the transition from $m_F=-4$ to $m_F=-3$ moves from the 'stationary' to the 'motion' state.

The linear polarizations of the two beams that create the lattice in a given direction are initially aligned, so the two states are trapped nearly identically. When the polarization of one of the lattice beams is rotated (using two electro-optic modulators and a $\lambda/4$ plate, where λ is the wavelength), the optical lattices for the two states move in opposite directions (see Fig. 1a). After rotating the polarization by π, we optically pump the atoms back to the stationary state and rotate the polarization back. The net effect of this sequence is that atoms that start in the stationary state move but return to the same place, while atoms that start in the motion state are shifted by one lattice site.

The sorting algorithm for compacting atoms in the lattice was proposed in previous work[15,21]; we have slightly modified it to allow the filling of any continuous sublattice (see Methods). The general idea is to first perform a series of balancing steps in the x and y directions so that every row in the z direction has the required number of atoms to fill a desired number of planes. Then, a series of compaction steps in the z direction moves atoms to fill the planes of the target sublattice (Fig. 1b). For example, to fill a $5 \times 5 \times 2$ sublattice from a half-filled $5 \times 5 \times 5$ lattice, atoms are first 'balanced' in the x and y directions so that every row in the z direction has at least two atoms. Parallel z-motion steps then move the atoms to the desired planes. After sorting, we reimage the atoms and repeat the procedure to correct any errors. The ability to know exactly where the vacancies are is an advantage of this approach to filling a lattice compared to implementing a superfluid–Mott insulator transition[22], where residual occupancy errors are unknown.

Figure 2 shows two implementations of this algorithm, in which target sublattices were completely filled after two sorts. In general, starting with at least half the lattice sites filled in a $5 \times 5 \times 5$ array, three sorts leave us with an average filling fraction of 0.97 for $5 \times 5 \times 2$ and 0.95 for $4 \times 4 \times 3$. We achieve the perfect filling shown in Fig. 2f and Fig. 2c 32% and 27% of the time, respectively. For the first sort, the

[1]Department of Physics, The Pennsylvania State University, University Park, PA, USA. *e-mail: dsweiss@phys.psu.edu

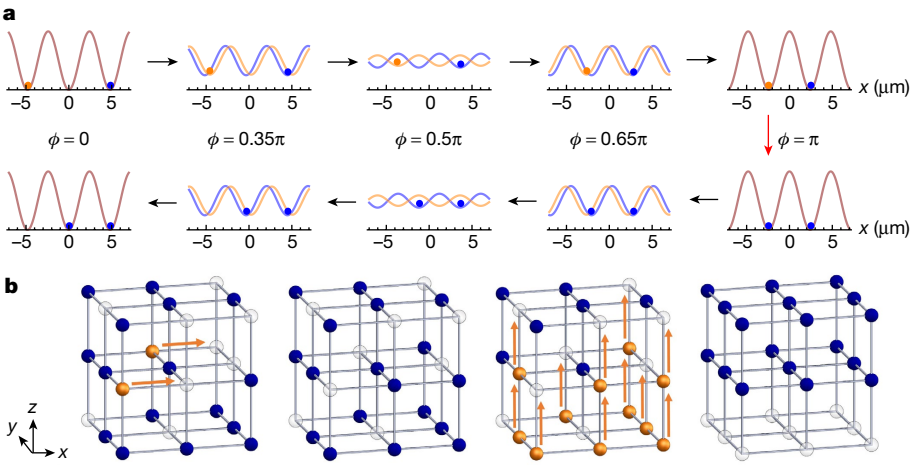

Fig. 1 | Motion steps and sorting algorithm. a, Motion steps used to fill a vacancy in a given direction. The curves show the lattice potential as a function of position for the 'motion' state (orange curve) and the 'stationary' state (blue curve). Brown curves indicate overlapping potentials. The arrows denote the direction of a time series in which the angle (ϕ) between the polarizations of the two lattice beams is adiabatically ramped to π and back to 0. The atom to be moved is transferred to the motion state (orange circle) using targeted addressing at the beginning of the time series. As the polarization of one of the lattice beams is rotated, the atoms in the motion state and the stationary state (blue circle) move in opposite directions, settling half a lattice spacing away from their original positions when $\phi = \pi$. The atom in the motion state is then optically pumped to the stationary state (illustrated by the red arrow). As the polarization is rotated back, both atoms move in the same direction, with the atom that started in the stationary state returning to its original position and the atom that started in the motion state moving by one lattice site. **b**, Simplified illustration of two parts of the sorting algorithm in a $3 \times 3 \times 3$ lattice. Orange and blue circles are as in **a**; empty circles denote empty sites. The first motion step 'balances' the array so that every z row has exactly two atoms. The second motion step 'compacts' atoms into two planes.

average number of motion steps is 6.4 (5.6) and the average number of addressing operations was 38 (62) for filling a $5 \times 5 \times 2$ ($4 \times 4 \times 3$) sublattice. Each sort takes about 190 ms on average. Figure 3 shows the filling fraction as a function of the number of sorts. These numbers match well with Monte Carlo simulations that consider measured sources of error (see Methods). A major source of error for atoms in both the motion and stationary states is spontaneous emission from the lattice. The spontaneous emission rate is significantly higher (17 times on average) during a motion step because the lattice intensity is not zero at the trap minima during the motion (see Fig. 1a). When an atom spontaneously emits a photon and changes hyperfine state, it becomes anti-trapped and is lost. The measured average loss per motion step is about 4×10^{-3}. Another source of error is imperfect transfer of atoms from the stationary state to the motion state. Our measured transfer fidelity is 0.986, limited by a combination of imperfect addressing beam shape, pointing noise of the addressing beams and magnetic field fluctuations. This error can cause two atoms to end up in the same lattice site, both of which are lost during imaging. The number of sorts that can be performed to fill errors is eventually limited by the 92-s vacuum lifetime and by double-atom loss. Optical pumping leads to a modest amount of heating, exciting about 7% of the population from the 3D vibrational ground state per motion step. Were we to replace the more convenient optical pumping with targeted addressing, this number would be reduced to 0.6%.

After sorting and a final round of projection cooling, we measure the vibrational sidebands to determine the final ground-state occupation, as shown in Fig. 4. Projection sideband cooling (see Methods) leads to ground-state occupation probabilities of 0.949(7), 0.954(6) and 0.985(1) in the x, y and z directions, respectively, which implies 89% occupation of the 3D vibrational ground state. The state is not thermal, but most of the population is in the lowest three levels. We calculate that the vibrational entropy for this state is about $0.59k_B$ per particle, where k_B is the Boltzmann constant.

The configurational entropy is given by[23]

$$S = \frac{1}{\overline{n}}\left[\overline{n}\ln\left(\frac{1}{\overline{n}}\right) + (1-\overline{n})\ln\left(\frac{1}{1-\overline{n}}\right)\right] \quad (1)$$

where $\overline{n}$ is the filling fraction. The solid blue line in Fig. 3 shows the configurational entropy as a function of the number of sorts, and the dotted line shows the vibrational entropy after projection cooling. Sorting reduces the configurational entropy by a factor of 8 and the total entropy by a factor of 2.44. The final total entropy per particle is $0.75k_B$.

The number of required motion steps scales as $N^{1/3}$, where N is the number of atoms to be sorted[15,21]. Similar scaling for state flipping could be obtained if the addressing beams were generated holographically; such a versatile 3D light pattern would allow many atoms to be state-flipped with microwaves simultaneously. Monte Carlo simulations using our current sequential addressing scheme and error rate show that starting from a half-filled $10 \times 10 \times 10$ lattice, $10 \times 10 \times 4$ and $7 \times 7 \times 7$ sublattices can be filled to a filling fraction of about 0.93. The error due to the motion could be reduced by further detuning the lattice light. Tripling the lattice detuning would decrease the spontaneous emission rate by a factor of 9 and the lattice depth by a factor of 3. Although the resulting lower trap frequency would require that we move atoms three times more slowly, the total spontaneous emission per motion step would be reduced by a factor of three, which would improve the filling fraction to approximately 0.975 for about 400 sorted atoms. It should be possible to improve microwave transfer errors by an order of magnitude by improving magnetic field stabilization and adapting our phase gate[14], which is insensitive to addressing-beam intensity fluctuations. Because atoms in a 3D lattice geometry have many near neighbours, small known filling errors can be readily incorporated into the design of any quantum computation.

We now more fully discuss our characterization of this experiment as the first, to our knowledge, to capture the full essence of Maxwell's demon on a large array of particles. Any process that involves selectively acting on particles differently depending on their momentum, energy or internal state, like all laser-cooling methods[5,24,25], evokes an aspect of Maxwell's demon, who sorted particles based on velocity. However, when there is no stored information, such mechanisms differ in spirit from Maxwell's demon and other thought-experiment demons[26]. When the entropy increase of the outside world is built into the cooling cycle, carried away by lost particles or scattered light, there is no trace of the

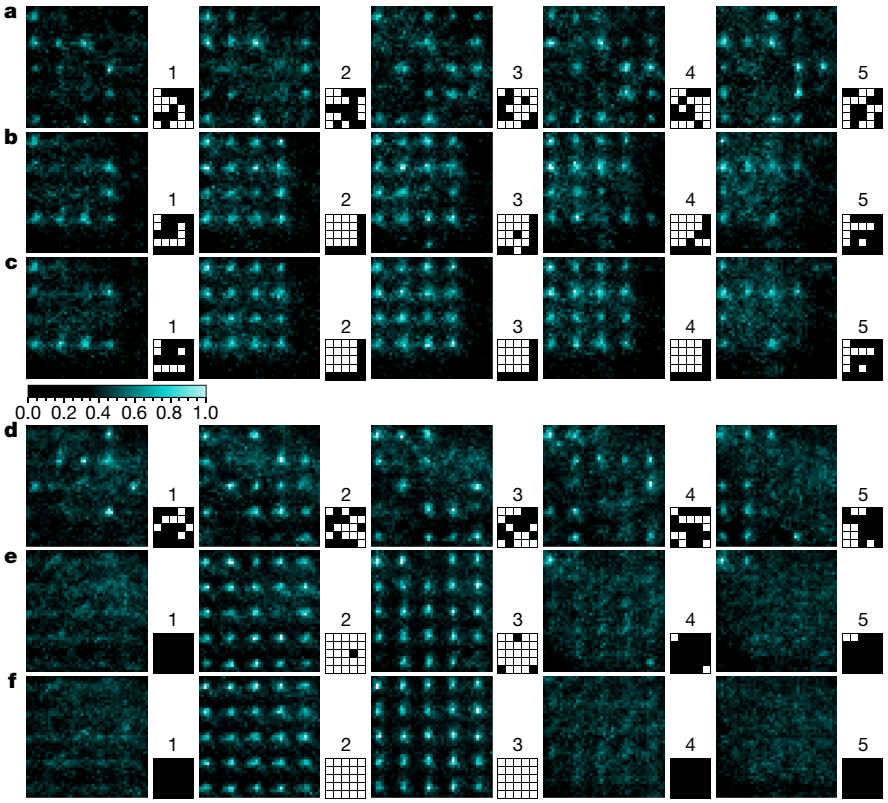

Fig. 2 | Perfect filling of 4 × 4 × 3 and 5 × 5 × 2 sublattices. a–f, The five images in each row correspond to the five lattice planes (labelled 1–5). The colour map shows intensity. We have applied contrast enhancement (a threshold of ~35% of the peak intensity) to make empty sites more obvious in the figure. The associated grid patterns are real-time occupancy maps, generated by processing the five images. The two sets of images (**a**–**c** and **d**–**f**) are from two different experimental implementations. **a**, An initial, unsorted atom distribution. The occupancy maps are used as the basis of a series of site-selective state flips and state-selective translations that execute our sorting algorithm. **b**, Result after one sorting sequence with the goal of filling a 4 × 4 × 3 sublattice in planes 2–4. There are three errors after this sort (one in plane 3, two in plane 4). **c**, Result after a second sorting sequence starting from the distribution in **b**. The sorting goal has been reached. Atoms outside the target sublattice can be kept as spares, or they can be selectively state-flipped and removed by a resonant clearing beam. **d**, Another initial, unsorted atom distribution. **e**, The result after one sorting sequence with the goal of filling a 5 × 5 × 2 sublattice in planes 2 and 3. There are four errors after this sort (one in plane 2, three in plane 3). **f**, The result after a second sorting sequence starting from the distribution in **e**. The sorting goal has been reached. The absence of spare atoms in **f** is coincidental.

theoretical paradox that twentieth-century information theory worked to resolve[2].

By contrast, our experiment is conceptually similar to Maxwell's thought experiment. We increase the entropy of the outside world in the process of determining site occupancy. At the same time, the configurational entropy goes to zero because there is only one state with that particular configuration. The stored occupancy information is then used as a guide to the execution of reversible operations that leave the system in a manifestly low-entropy state. Of course, that is also true for any sorting operation, as when checkers are arrayed on a board. The difference here is that most of the initial entropy of our system is in the initial configurational disorder, so that by measuring and sorting we considerably reduce the total system entropy. Maxwell's demon collected information and acted on one particle at a time. By contrast, our demon obtains an occupancy map of the whole system, so that it can map out a plan to act on all the particles in parallel.

Maxwell visualized work being extracted from the reconfigured system by using the demon-imposed temperature gradient to drive a heat engine. Work can probably not be extracted in our experiment, but the fact that the overall system entropy is reduced means that trap changes that affect all atoms in the same way can create a much colder gas. For instance, the experiment would pass the $1.24k_B$ entropy-per-particle threshold below which there would be a Bose–Einstein condensate if the lattice were adiabatically shut off and the atoms were

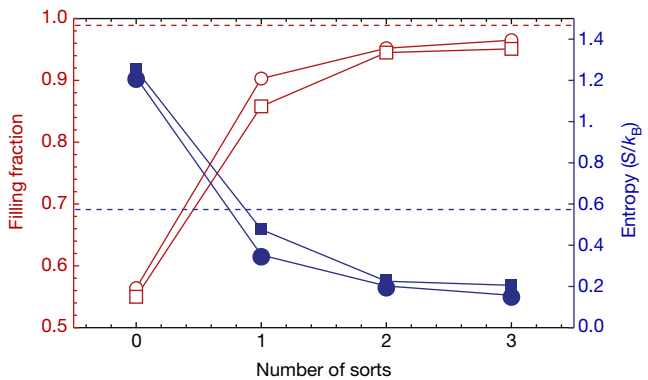

Fig. 3 | Filling fraction and entropy. The empty red symbols show the filling fraction as a function of the number of sorts for 5 × 5 × 2 (circles) and 4 × 4 × 3 (squares) target sublattices. The circles (squares) show results based on 85 (48) experimental implementations. The red horizontal dashed line is the limit associated with loss from collisions with background gas atoms during the 1 s required to image and sort. The solid blue symbols show the configurational entropy as a function of the number of sorts for 5 × 5 × 2 (circles) and 4 × 4 × 3 (squares) target sublattices. The total entropy at the beginning and at the end is the sum of the vibrational entropy (blue horizontal dotted line) and the configurational entropy; sorting reduces it by a factor of 2.44. The 1σ error bars are smaller than the size of the symbols.

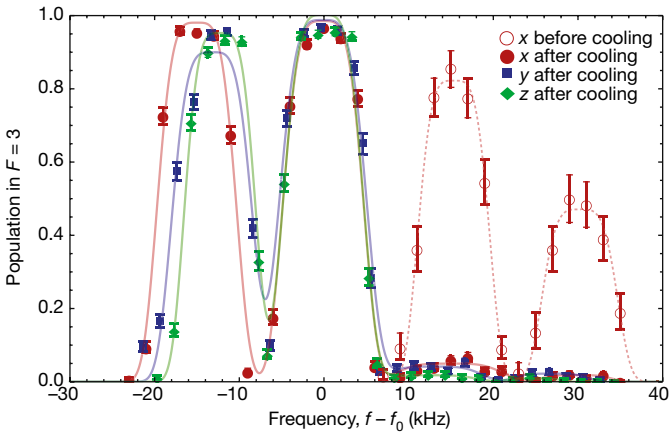

Fig. 4 | Microwave spectra showing the results of projection sideband cooling[18]**.** Atoms start in $|F=4, m_F=-4\rangle$, and the curves show the number of atoms that make an adiabatic fast-passage transition from the $|F=4, m_F=-4\rangle$ to the $|F=3, m_F=-3\rangle$ state because atoms that remain in $|F=4, m_F=-4\rangle$ are cleared by a resonant beam before detection. Slightly rotating the polarization of one lattice beam of the x, y or z lattice beam pairs leads to non-zero projections between different vibrational states (vibrational quantum number ν) in that direction. Nearly all atoms make the transition at the peaks centred at zero, where the frequency is $f=f_0\approx 9.19130$ GHz, which corresponds to no change of vibrational level. Nearly all atoms make the transition at the lower-frequency peaks (at $f-f_0\approx -15$ kHz), which corresponds to the vibrational quantum number increasing by one ($\Delta\nu=+1$). Atoms make the transition at the higher-frequency peaks ($\Delta\nu=-1$, at $f-f_0\approx 15$ kHz) only if there is a lower vibrational level available, which is true for all atoms except those in the vibrational ground state. The heights of the $\Delta\nu=-1$ peaks thus provide a measure of the atoms that are not in the vibrational ground state. The empty maroon circles show the $\Delta\nu=-1$ and $\Delta\nu=-2$ sidebands in the x direction before projection sideband cooling. The sidebands for the y and z directions are similar (not shown). The solid maroon circles, solid blue squares and solid green diamonds show the spectra for the x, y and z directions, respectively, after projection sideband cooling. Each data point in the 'before cooling' dataset is obtained from about 60 atoms and in the 'after cooling' datasets from about 400 atoms. All error bars represent one standard deviation. The maroon, blue and green solid lines are sums of four fitted super-Gaussians of order 4 for the x, y and z directions, respectively. We infer from the large suppressions of the $\Delta\nu=-1$ and $\Delta\nu=-2$ sidebands in this figure that the 3D vibrational ground state is occupied 88.9(9)% of the time.

left in a 3D box potential[23,27]. The adiabatic timescale for making this approximate Mott-insulator-to-superfluid transition is far too large given our current lattice spacing, but it could be accomplished if the lattices were made in an accordion configuration[28], in which the angle between the beam pairs could be dynamically changed to reduce the lattice constant by a factor of five. That would present a third path to quantum degeneracy of cold atoms, joining many evaporative-cooling experiments and one laser-cooling experiment[25,29].

Maxwell's thought experiment led to a deep understanding of the relationship between entropy and information. The experiment that we present here has several practical applications. It prepares a favourable initial state for a neutral-atom quantum computer with one atom at nearly every 3D lattice site, each cooled near its vibrational ground state. The cold array minimizes many potential errors in Rydberg-gate-based quantum computations. The 3D optical lattice allows entanglement with many near neighbours and provides favourable scaling, often as $N^{1/3}$ or $N^{2/3}$, to minimize computation time and the laser power requirements. If we can further improve cooling—for instance, by temporarily transferring the atoms to a lattice with smaller detuning, where the atoms are trapped more deeply in the Lamb–Dicke limit—we might be able to create large-scale entanglement through cold-collision gates[30,31] and thus ultimately implement one-way quantum computation[32]. Our sorted array could also be used for a variety of Rydberg-based quantum simulations with different geometries, dimensionalities and anisotropy of interactions. For instance, the simulations of Ising-like Hamiltonians that have recently been implemented in one- and two-dimensional (2D) tweezer and microtrap arrays[16,33] could be extended to three dimensions in our optical lattice. Our demonstrated coherent site-selective control[14] allows the possible implementation of a universal quantum simulator, which might be used to implement Kitaev's toric code in 2D sublattices and in 2D or 3D lattice gauge theories[34].

Online content

Any methods, additional references, Nature Research reporting summaries, source data, statements of data availability and associated accession codes are available at https://doi.org/10.1038/s41586-018-0458-7.

Received: 15 January 2018; Accepted: 16 July 2018;
Published online 5 September 2018.

1. Maxwell, J. C. *Theory of Heat* (Longmans, Green and Co., London, 1871).
2. Leff, H. S. & Rex, A. F. *Maxwell's Demon: Entropy, Information, Computing* (Princeton University Press, Princeton, 1990).
3. Brillouin, L. Maxwell's demon cannot operate – information and entropy. 1. *J. Appl. Phys.* **22**, 334–337 (1951).
4. Landauer, R. Irreversibility and heat generation in the computing process. *IBM J. Res. Dev.* **5**, 183–191 (1961).
5. Price, G. N., Bannerman, S. T., Viering, K., Narevicius, E. & Raizen, M. G. Single-photon atomic cooling. *Phys. Rev. Lett.* **100**, 093004 (2008).
6. Barredo, D., de Leseleuc, S., Lienhard, V., Lahaye, T. & Browaeys, A. An atom-by-atom assembler of defect-free arbitrary two-dimensional atomic arrays. *Science* **354**, 1021–1023 (2016).
7. Endres, M. et al. Atom-by-atom assembly of defect-free one-dimensional cold atom arrays. *Science* **354**, 1024–1027 (2016).
8. Robens, C. et al. Low-entropy states of neutral atoms in polarization-synthesized optical lattices. *Phys. Rev. Lett.* **118**, 065302 (2017).
9. Lester, B. J., Luick, N., Kaufman, A. M., Reynolds, C. M. & Regal, C. A. Rapid production of uniformly filled arrays of neutral atoms. *Phys. Rev. Lett.* **115**, 073003 (2015).
10. Strasberg, P., Schaller, G., Brandes, T. & Esposito, M. Thermodynamics of a physical model implementing a Maxwell demon. *Phys. Rev. Lett.* **110**, 040601 (2013).
11. Barredo, D., Lienhard, V., de Léséleuc, S., Lahaye, T. & Browaeys, A. Synthetic three-dimensional atomic structures assembled atom by atom. *Nature* http://dx.doi.org/10.1038/s41586-018-0450-2 (2018).
12. Kim, H. et al. In situ single-atom array synthesis using dynamic holographic optical tweezers. *Nat. Commun.* **7**, 13317 (2016).
13. Saffman, M. Quantum computing with atomic qubits and Rydberg interactions: progress and challenges. *J. Phys. B* **49**, 202001 (2016).
14. Wang, Y., Kumar, A., Wu, T. Y. & Weiss, D. S. Single-qubit gates based on targeted phase shifts in a 3D neutral atom array. *Science* **352**, 1562–1565 (2016).
15. Weiss, D. S. et al. Another way to approach zero entropy for a finite system of atoms. *Phys. Rev. A* **70**, 040302 (2004).
16. Bernien, H. et al. Probing many-body dynamics on a 51-atom quantum simulator. *Nature* **551**, 579–584 (2017).
17. Nelson, K. D., Li, X. & Weiss, D. S. Imaging single atoms in a three-dimensional array. *Nat. Phys.* **3**, 556–560 (2007).
18. Li, X., Corcovilos, T. A., Wang, Y. & Weiss, D. S. 3D projection sideband cooling. *Phys. Rev. Lett.* **108**, 103001 (2012).
19. Wang, Y., Zhang, X. L., Corcovilos, T. A., Kumar, A. & Weiss, D. S. Coherent addressing of individual neutral atoms in a 3D optical lattice. *Phys. Rev. Lett.* **115**, 043003 (2015).
20. Deutsch, I. H. & Jessen, P. S. Quantum-state control in optical lattices. *Phys. Rev. A* **57**, 1972–1986 (1998).
21. Vala, J. et al. Perfect pattern formation of neutral atoms in an addressable optical lattice. *Phys. Rev. A* **71**, 032324 (2005).
22. Jaksch, D., Bruder, C., Cirac, J. I., Gardiner, C. W. & Zoller, P. Cold bosonic atoms in optical lattices. *Phys. Rev. Lett.* **81**, 3108–3111 (1998).
23. Olshanii, M. & Weiss, D. Producing Bose–Einstein condensates using optical lattices. *Phys. Rev. Lett.* **89**, 090404 (2002).
24. Chu, S., Hollberg, L., Bjorkholm, J. E., Cable, A. & Ashkin, A. Three-dimensional viscous confinement and cooling of atoms by resonance radiation pressure. *Phys. Rev. Lett.* **55**, 48–51 (1985).
25. Anderson, M. H., Ensher, J. R., Matthews, M. R., Wieman, C. E. & Cornell, E. A. Observation of Bose–Einstein condensation in a dilute atomic vapor. *Science* **269**, 198–201 (1995).
26. Szilard, L. Über die Entropieverminderung in einem thermodynamischen System bei Eingriffen intelligenter Wesen. *Z. Phys.* **53**, 840–856 (1929).
27. Gaunt, A. L., Schmidutz, T. F., Gotlibovych, I., Smith, R. P. & Hadzibabic, Z. Bose–Einstein condensation of atoms in a uniform potential. *Phys. Rev. Lett.* **110**, 200406 (2013).
28. Williams, R. A. et al. Dynamic optical lattices: two-dimensional rotating and accordion lattices for ultracold atoms. *Opt. Express* **16**, 16977–16983 (2008).
29. Hu, J. Z. et al. Creation of a Bose-condensed gas of Rb-87 by laser cooling. *Science* **358**, 1078–1080 (2017).

30. Jaksch, D., Briegel, H. J., Cirac, J. I., Gardiner, C. W. & Zoller, P. Entanglement of atoms via cold controlled collisions. *Phys. Rev. Lett.* **82**, 1975–1978 (1999).
31. Kaufman, A. M. et al. Entangling two transportable neutral atoms via local spin exchange. *Nature* **527**, 208–211 (2015).
32. Raussendorf, R. & Briegel, H. J. A one-way quantum computer. *Phys. Rev. Lett.* **86**, 5188–5191 (2001).
33. Labuhn, H. et al. Tunable two-dimensional arrays of single Rydberg atoms for realizing quantum Ising models. *Nature* **534**, 667–670 (2016).
34. Weimer, H., Muller, M., Lesanovsky, I., Zoller, P. & Buchler, H. P. A Rydberg quantum simulator. *Nat. Phys.* **6**, 382–388 (2010).

Acknowledgements This work was supported by the US National Science Foundation through grant PHY-1520976.

Author contributions All authors contributed to the design, execution and analysis of the experiment and the writing of the manuscript. A.K., T.-Y.W. and F.G. collected all the data.

Competing interests The authors declare no competing interests.

Additional information
Extended data is available for this paper at https://doi.org/10.1038/s41586-018-0458-7.
Reprints and permissions information is available at http://www.nature.com/reprints.
Correspondence and requests for materials should be addressed to D.S.W.
Publisher's note: Springer Nature remains neutral with regard to jurisdictional claims in published maps and institutional affiliations.

METHODS

Apparatus. We load atoms from a Magneto-Optical Trap to a 3D optical lattice formed by three pairs of 75-μm-waist, 838.95-nm laser beams. Each lattice beam has a power of 250 mW, giving a lattice depth of 190 μK at the central lattice site. The two beams in each pair cross each other at 10°, yielding a lattice spacing of 4.9 μm. Two pairs are frequency-shifted relative to the third by +30 MHz and −175 MHz to prevent mutual interference among the lattice pairs. One beam in each pair has two electro-optic modulators in its path, aligned so that their axes are at 45° relative to the incoming polarization, followed by a $\lambda/4$ wave-plate aligned with the incoming polarization. As the voltage on the electro-optic modulators is increased, the polarization of this beam rotates. The angle of rotation is π when the half-wave voltage is applied to both electro-optic modulators.

Projection sideband cooling. Projection sideband cooling has been described in detail in a previous paper[18]. We give a brief overview here. Projection sideband cooling is similar to other sideband-cooling techniques, except that microwave photons, which have a very small momentum compared to the optical photons that are usually used, drive the vibrational-state-changing transitions. To accomplish this, for a given lattice direction, say x, the polarization of one of the lattice beams in the pair is rotated slightly, which displaces the traps experienced by atoms in the $|F=4, m_F=-4\rangle$ and $|F=3, m_F=-3\rangle$ states slightly relative to each other (the same effect that we use to state-selectively translate atoms during our sorting operations). Therefore, all the vibrational wavefunctions associated with one magnetic sublevel have non-zero projections onto the wavefunctions of the other sublevel. There are consequently non-zero matrix elements for vibration-state-changing microwave transitions.

Projection cooling proceeds as follows. All the atoms are prepared in $|F=4, m_F=-4\rangle$ via optical pumping. The x lattice-beam polarization is rotated, and then a $\Delta\nu_x=-2$ microwave adiabatic fast passage (AFP) pulse drives the transition $|F=4, m_F=-4\rangle$ to $|F=3, m_F=-3\rangle$, followed by a modified polarization rotation and then a $\Delta\nu_x=1$ microwave pulse from $|F=3, m_F=-3\rangle$ to $|F=4, m_F=-4\rangle$ (which is a $\Delta\nu=-1$ pulse for atoms that start in $|F=4, m_F=-4\rangle$). The AFP pulses work well regardless of the initial vibrational state. The two AFP pulses lower ν_x by 1 for all the atoms except those initially in $\nu_x=0$, which make no transitions. All the atoms for which both AFP pulses were successful end in $|F=4, m_F=-4\rangle$, except those that started in $\nu_x=1$. The polarization is rotated back, and an optical pumping pulse resets all the atoms to $|F=4, m_F=-4\rangle$. These steps are then repeated for the y and z lattice beams, and then the sequence is repeated 50 times. The whole cooling sequence takes about 1 s. The $\Delta\nu=-2\rightarrow\Delta\nu=1$ sequences minimize the number of times that an atom has to be optical pumped, which is a particular advantage for cooling atoms from high vibrational states. Sequentially stepping through the Cartesian directions optimizes the final cooling steps.

We have improved the performance of our previously demonstrated projection sideband cooling method[18] considerably, from 76% to 89% occupancy of the ground vibrational state. This improvement results from two changes. First, we increased the fidelity of the $\Delta\nu=-2$ microwave pulse, where $\Delta\nu$ is the microwave-driven change in vibrational level, by separately optimizing the lattice displacement for $\Delta\nu=-2$ and $\Delta\nu=-1$. Second, we improved the quality of the optical-pumping-light polarization at the atoms by a factor of 5.

Implementation of a motion step. Extended Data Fig. 1 illustrates our timing sequence for one motion step. Before any motion, atoms are optically pumped to the $|F=4, m_F=-4\rangle$ state (not shown). The atoms to be moved are transferred to the $|F=3, m_F=-3\rangle$ state sequentially. The addressing lasers, directed by micro-mechanical electronic systems mirrors, cross at a target atom in the 3D array, causing an a.c. Stark shift on its resonance frequency between $|F=4, m_F=-4\rangle$ and $|F=3, m_F=-3\rangle$ by −50 kHz with respect to the atoms that are not in the path of either addressing laser. The addressing laser powers are ramped up over 40 μs, after which we wait for another 110 μs for our intensity lock to settle. We drive the transition in the target atoms with a 3-ms-long AFP microwave pulse, which involves a 12-kHz frequency sweep. The crosstalk is less than 3×10^{-3}.

To initiate motion, the polarization of one of the lattice beams is linearly rotated by π over 3 ms by ramping the voltages on the electro-optic modulators. The atoms in $|F=3, m_F=-3\rangle$ are then optically pumped to $|F=4, m_F=-4\rangle$ in 0.2 ms (with an intensity of 4 mW cm^{-2} and detuning of −7.5 MHz on the $F=3$ to $F'=4$ transition, and 0.5 mW cm^{-2} and 7.5 MHz on the $F=4$ to $F'=4$ transition). The voltages are then ramped back to zero. A final optical pumping step over 0.25 ms ensures that all atoms are back to $|F=4, m_F=-4\rangle$ for the next motion step.

Measuring state-flip fidelity. To measure the efficiency of our addressing scheme, we take an occupancy map, apply projection sideband cooling to the atoms and optically pump them to the $|F=4, m_F=-4\rangle$ state. We then sequentially flip the state of all the atoms within a $5\times5\times5$ region to $|F=3, m_F=-3\rangle$ using targeted addressing. Then, another laser beam resonant with the transition from $|F=4\rangle$ to $|F'=5\rangle$ pushes away the atoms that were left in the $|F=4, m_F=-4\rangle$ state. A new occupancy map is then generated to identify the atoms that were successfully transferred to $|F=3, m_F=-3\rangle$. Averaging over 50 implementations, we measure a state-flip fidelity of 0.986(5). However, the addressing laser beam drifts slowly once aligned, which can decrease the state-flip fidelity by about 0.02 after about 100 sorting operations.

Measuring motion fidelities. Motion errors can occur when atoms spontaneously emit lattice light. An atom is usually lost during motion if light scattering leaves it in the anti-trapped state. Occasionally the atom site-hops, if it stays trapped but follows the 'wrong' lattice potential. We measured the motion fidelities for atoms in $|F=4, m_F=-4\rangle$ and $|F=3, m_F=-3\rangle$ separately (see Extended Data Fig. 2). Atoms were first projection-sideband-cooled and optically pumped to $|F=4, m_F=-4\rangle$. To find the cumulative effect of making $2N$ motion steps in a given direction, we ramped up to the half-wave voltage, $V_{\lambda/2}$, of the electro-optic modulators, then ramped down to $-V_{\lambda/2}$, and repeated the process N times. Because no optical pumping or state flips were applied during the motions, all the atoms moved back and forth by one lattice spacing around their initial positions. By comparing the occupancy maps before and after these motions steps, we can identify the percentage of atoms that successfully return to their initial positions, which we call the motion fidelity. For motion in $|F=3, m_F=-3\rangle$, the sequence is the same except that after the atoms are optically pumped to $|F=4, m_F=-4\rangle$, a global microwave pulse is applied to flip the state of all atoms to $|F=3, m_F=-3\rangle$ before executing the motions. Each data point in Extended Data Fig. 2 is averaged over 10 sorting operations and corrected for the loss due to collisions with background gas atoms. A linear fit gives the fidelities per motion step. For atoms in the $|F=4, m_F=-4\rangle$ state and motion in the lattice directions, the fidelities are {0.9951(6), 0.9982(6), 0.9962(4)}, where the errors refer to one standard deviation. The corresponding fidelities for atoms in the $|F=3, m_F=-3\rangle$ state are {0.9956(4), 0.9961(10), 0.9956(1)}. The calculated probability of spontaneous emission for an atom in the vibrational ground state during a motion step is 3.5×10^{-3}.

Sorting algorithm. We have generalized the sorting algorithm for any initial $N\times N\times N$ lattice and any final $i\times j\times k$ sublattice. If $i=j=N$, then only balancing and compaction steps are needed. If $i, j<N$, then extra motion steps in x and y are added to move as many atoms as possible into an $i\times j\times N$ sublattice from 'outside' before balancing and compaction ('outside' means the full lattice minus the target sublattice). For example, to fill a $4\times4\times3$ sublattice, as many atoms as possible are first moved into a $4\times4\times5$ region in two motion steps, one in x and one in y, from outer y–z and x–z planes of the lattice. Balancing and compaction are then applied to a $4\times4\times5$ lattice rather than a $5\times5\times5$ lattice. The simulations that we describe below suggest that even though this procedure does not always empty the outside planes, there are always enough atoms to fill a $4\times4\times3$ sublattice when starting from a 50% filled $5\times5\times5$ lattice.

The steps for balancing an $i\times j\times N$ lattice to fill an $i\times j\times k$ sublattice are roughly as follows:

1. If this is the first iteration, choose a dividing plane, P, to be an x–z plane. Otherwise, choose the dividing plane to be perpendicular (either x–z or y–z) to the previous iteration. Choose P to divide the lattice into two parts, S_1 and S_2, that are as similar as possible (that is, a difference of one plane between S_1 and S_2 is permitted if the lattice dimension is odd).
2. If the number of z rows in S_1 (S_2) is n (m), the required number of atoms in S_1 (S_2) is $k\times n$ ($k\times m$). Move atoms between the two sublattices until they each have at least the required number of atoms.
3. Repeat these steps for S_1 and S_2 separately, stopping when each of them is just a single z row.

Balancing guarantees that there are k atoms in each of the $i\times j$ z rows. These atoms are then moved in the z direction ('compaction') in parallel to fill the desired k planes, usually in the middle of the accessible lattice. The algorithm minimizes the number of motion steps.

The sorting algorithm can probably be improved by replacing the initial steps to empty the outer x–z and y–z planes by a more optimal algorithm. For instance, the first sort could be modified to distribute the extra atoms evenly and thus reduce the number of correction steps.

Monte Carlo simulations. Monte Carlo simulations of this sorting algorithm start with a randomly half-filled 3D array. Errors are probabilistically applied at each motion step and atom loss is considered after the completion of a sort. We calculate a separate motion fidelity for each internal state as the average of the measured fidelities in the three directions. One thousand simulations were run for various lattice dimensions and various target sublattices. For filling a $5\times5\times2$ or $4\times4\times3$ sublattice from a half-filled $5\times5\times5$ lattice, the simulations predict an average filling factor of about 0.97 after three sorts, in agreement with our measured filling factor to within the uncertainty associated with our measured errors.

Real-time control. The sorting process requires changing the timing sequence in real time. This is accomplished by combining real-time data analysis with two field-programmable gate arrays (FPGAs). The experiment has a 'backbone' of a fixed timing sequence. After the motion steps have been generated according to the initial occupancy map, the FPGAs pause that fixed timing sequence and take

control of the electronic channels (optical pumping, electro-optic modulator voltages, addressing, microwaves) required for sorting. The data used for sorting, which comprise a sequence of directions for the motion steps and the lattice sites to be addressed at each motion step, are communicated to the FPGAs by the program that generates the occupancy map and creates the sorting plan. The FPGAs convert the motion steps into several voltage sequences that are output synchronously. After the motion steps have been executed, the FPGAs transfer the timing control back to the fixed backbone, which resumes where it was paused.

Code availability. The Monte Carlo code used to model our algorithm is available from the corresponding author on request.

Data availability. The underlying data used to generate the figures and conclusions in the paper are available from the corresponding author on reasonable request.

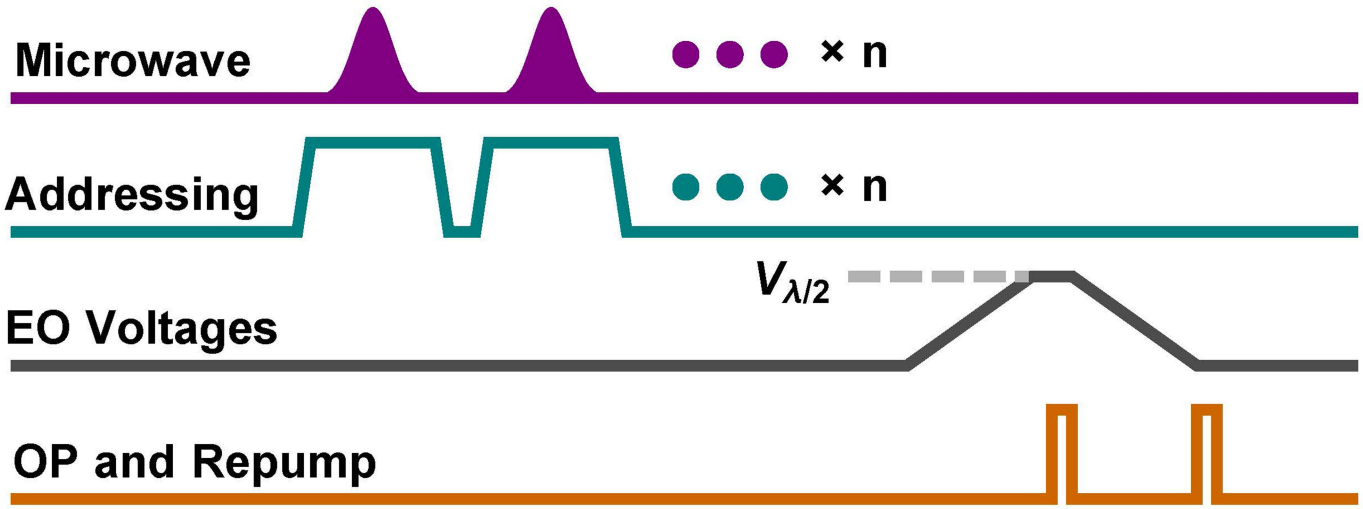

Extended Data Fig. 1 | Motion step. A motion step to move *n* atoms is shown. *n* atoms are sequentially targeted by the addressing beams and transferred from the 'stationary' state to the 'motion' state using microwaves. The electro-optic modulator (EO) voltages are ramped up to the half-wave voltage ($V_{\lambda/2}$) in order to move atoms by half of the lattice spacing. After motion, the atoms are optically pumped so that they all return to the stationary state. The EO voltages are then ramped back down. A final optical pumping (OP) ensures optimal preparation for the next motion step.

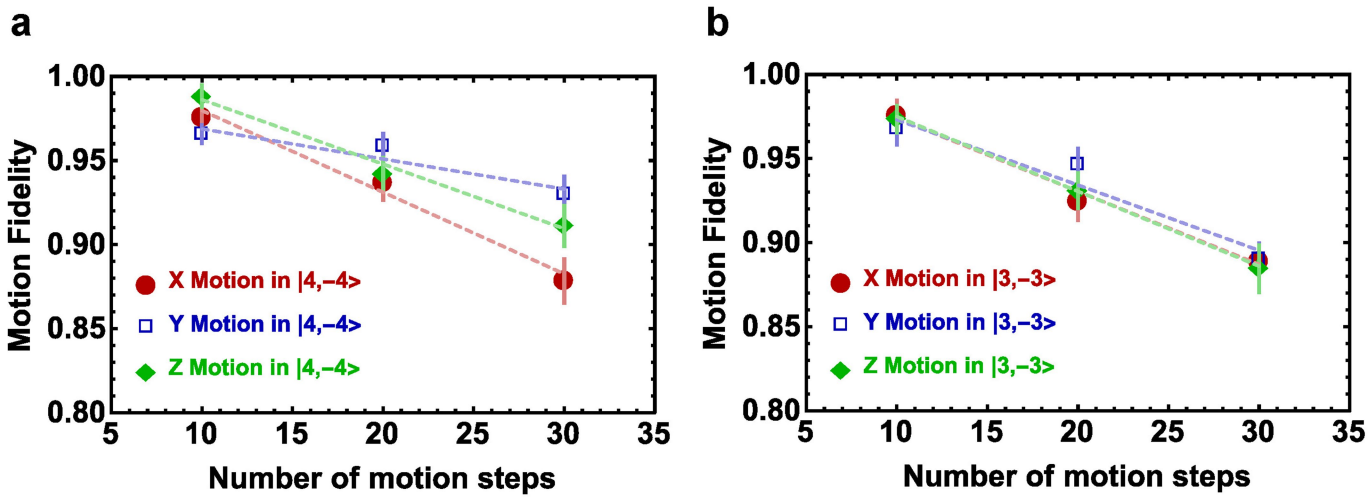

Extended Data Fig. 2 | Motion fidelities. a, **b**, Measured motion fidelity as a function of the number of motion steps in $|F = 4, m_F = -4\rangle$ (**a**) and $|F = 3, m_F = -3\rangle$ (**b**) in the x (maroon circles), y (blue squares) and z (green diamonds) directions. The lines are fits to the data. The error bars represent one standard deviation. Each point corresponds to about 600 atoms.